NACA RM H56H08

NACA

RESEARCH MEMORANDUM

ANALYSIS OF THE VERTICAL-TAIL LOADS MEASURED DURING A FLIGHT INVESTIGATION AT TRANSONIC SPEEDS OF THE DOUGLAS X-3 RESEARCH AIRPLANE

By William L. Marcy, Harriet J. Stephenson,
and Thomas V. Cooney

High-Speed Flight Station
Edwards, Calif.

NATIONAL ADVISORY COMMITTEE
FOR AERONAUTICS

WASHINGTON

November 9, 1956
Declassified August 14, 1958

NATIONAL ADVISORY COMMITTEE FOR AERONAUTICS

RESEARCH MEMORANDUM

ANALYSIS OF THE VERTICAL-TAIL LOADS MEASURED DURING A FLIGHT INVESTIGATION AT TRANSONIC SPEEDS OF THE DOUGLAS X-3 RESEARCH AIRPLANE

By William L. Marcy, Harriet J. Stephenson, and Thomas V. Cooney

SUMMARY

Results are presented of an analysis of the strain-gage measurements of vertical-tail loads experienced in rudder pulses, gradually increasing sideslips, and rudder-fixed aileron rolls at transonic speeds with the Douglas X-3 research airplane. A Mach number range from approximately 0.7 to 1.2 at an altitude of about 30,000 feet was covered during this investigation.

The lift-curve slope of the vertical tail increased with increasing Mach number from a value of 0.038 per degree at a Mach number of 0.7 to a maximum of 0.048 per degree at a Mach number of 0.94, followed by a reduction to 0.041 at supersonic Mach numbers. A comparison with available methods of estimating this parameter indicated good agreement with flight results. The effectiveness of the rudder (lift-curve slope of the vertical tail due to deflecting the rudder) decreased from approximately 0.020 per degree at subsonic Mach numbers to 0.013 per degree at supersonic Mach numbers.

In several violent roll maneuvers, sideslip angles of as much as 21° were reached without stalling of the vertical tail, although vertical-tail effectiveness was reduced at sideslip angles above about 12°.

At sideslip angles below about 6° the center of pressure of the load on the vertical tail in sideslip was practically unchanged with Mach number, remaining at about 55 percent span and 30 percent chord. At sideslip angles above this value a more rearward center of pressure was indicated. The center of load due to displacing the rudder was farther inboard, 45 percent span, and farther rearward, 63 percent chord, than in sideslip, and moved rearward to 85 percent chord at supersonic Mach numbers.

The variation of airplane yawing-moment coefficient with sideslip, as determined from vertical-tail-loads measurements, increased from 0.0023 per degree at a Mach number of 0.7 to a maximum of 0.0032 at a Mach number of 0.94, and decreased to 0.0023 at supersonic Mach numbers.

INTRODUCTION

The configuration of the Douglas X-3 research airplane embodies several features of interest to designers at the present time, such as a long slender fuselage extending well forward of the airplane center of gravity, low-aspect-ratio unswept wings, and twin jet engines exhausting near the fuselage. Because of general interest in this type configuration and particular interest in the vertical-tail loads associated with maneuvering such aircraft, a flight investigation was undertaken at the NACA High-Speed Flight Station at Edwards, Calif., to obtain information on the loads encountered by the vertical tail in the transonic speed range.

Flight measurements were obtained in rudder-pulse and steady sideslip maneuvers and in aileron rolls in the Mach number range from about $M = 0.7$ to $M = 1.2$ at an altitude of about 30,000 feet. An analysis of the measured data was made in order to isolate such parameters as vertical-tail lift-curve slope, rudder effectiveness, and airplane yawing-moment coefficient due to sideslip. The results of the analysis are presented and comparisons with existing data are made where possible.

This investigation is a continuation of the Air Force-Navy-NACA joint effort, using special research aircraft as flight test vehicles, to investigate loads, performance, and stability at transonic and supersonic speeds. Results of several phases of the overall investigation with the X-3 airplane have been reported in references 1 to 6.

SYMBOLS

All derivatives, inertias, and airplane motions are referred to the body system of axes.

b wing span, ft

b_v vertical-tail-panel span (outboard of strain-gage station), ft

C_{b_v} vertical-tail-panel bending-moment coefficient, $\frac{M_v}{qs_v b_v}$

$\frac{dC_{b_V}}{dC_{Y_V}}$ spanwise center of load, percent b_V

C_{L_α} lift-curve slope, per deg

C_{n_β} yawing-moment coefficient due to sideslip of complete airplane

$C_{n_{\beta_V}}$ yawing-moment coefficient due to sideslip of vertical-tail panel

$C_{n_{\beta_{wf}}}$ yawing-moment coefficient due to sideslip of airplane less vertical tail

C_{T_V} vertical-tail-panel torque coefficient, $\frac{T_V}{qS_V\bar{c}}$

$\frac{dC_{T_V}}{dC_{Y_V}}$ chordwise center of load, percent $\bar{c}$

C_{Y_V} vertical-tail-panel side-force coefficient, $\frac{L_V}{qS_V}$

$\bar{c}$ mean aerodynamic chord of vertical-tail panel, ft

g acceleration due to gravity, ft/sec^2

I_X moment of inertia about X-axis, slug-ft^2

I_Y moment of inertia about Y-axis, slug-ft^2

I_Z moment of inertia about Z-axis, slug-ft^2

I_{XZ} product of inertia, slug-ft^2

L_V aerodynamic load on vertical-tail panel, lb

l_V distance between the airplane center of gravity and the quarter chord of the vertical-tail panel $\bar{c}$, ft

M free-stream Mach number

M_V vertical-tail panel aerodynamic bending moment about strain-gage station, ft-lb

p	rolling angular velocity, radians/sec
q	free-stream dynamic pressure, lb/sq ft
r	yawing angular velocity, radians/sec
$\dot{r}$	yawing angular acceleration, radians/sec^2
S	wing area, sq ft
S_v	vertical-tail-panel area, sq ft
T_v	vertical-tail-panel aerodynamic torque about the quarter chord of the panel $\bar{c}$, ft-lb
t	time, sec
α	airplane angle of attack, deg
β	angle of sideslip, deg
δ_a	total aileron deflection (sum of right and left), deg
δ_r	rudder deflection, deg

DESCRIPTION OF AIRPLANE

The Douglas X-3 is a single-place research airplane with 4.5-percent-thick modified hexagonal section low-aspect-ratio wing, and a long pointed fuselage. The wing is unswept at the 75-percent chord. The vertical-tail surface has a 4.5-percent-thick modified hexagonal section with quarter-chord line swept back 40°. The horizontal tail is located a distance of approximately half the depth of the fuselage below the vertical tail. All controls are actuated by an irreversible hydraulic power system incorporating artificial feel devices. The airplane is powered by two jet engines with afterburners that exhaust near the fuselage. Figure 1 is a photograph of the test airplane and a three-view drawing is shown in figure 2. Table I presents pertinent physical characteristics of the airplane.

INSTRUMENTATION AND ACCURACY

Standard NACA recording instruments were used to measure the following quantities pertinent to this investigation:

Airspeed and altitude
Angles of attack and sideslip
Normal, lateral, and longitudinal accelerations at the airplane center of gravity
Pitching, yawing, and rolling angular velocities at the airplane center of gravity
Control-surface positions

The error in Mach number based on a flight calibration of the airspeed system in the test airplane is estimated to be within ±0.01. Angle of attack and angle of sideslip, measured by vanes located on the nose boom, are considered for the test conditions encountered to be accurate to within ±0.5°. Increments in angle of sideslip, however, as used in the subsequent analysis of the measured data are considered to be accurate to ±0.1°. Lateral acceleration measurements pertinent to the present investigation are estimated to be accurate to ±0.01g; angular velocities in yaw, ±0.01 radian/sec; and in roll, ±0.03 radian/sec. Control-surface deflections were measured at the control surface and are estimated to be accurate to ±0.1°.

In addition to the standard instruments, strain gages were installed near the root of the vertical tail (see fig. 2) and were calibrated to indicate shear, bending moment, and torque. Based on the results of a calibration of the strain gages, and considering the accuracy with which the flight records could be read and the accuracy of inertia corrections which were applied to the structural loads, the estimated accuracy of the strain-gage results is ±100 pounds aerodynamic shear, and ±2,000 inch-pounds aerodynamic bending-moment and torque. When expressed in terms of load coefficients, these shear and moment accuracies result in an accuracy of approximately ±0.02 for C_{Y_V} and ±0.01 for C_{b_V} and C_{T_V} based on the dynamic pressure value corresponding to the lowest test Mach number.

TESTS

Maneuvers pertinent to this investigation of the X-3 airplane consisted of rudder pulses, gradually increasing sideslips, and rudder-fixed aileron rolls. The maneuvers were performed at an altitude of

about 30,000 feet and covered a Mach number range from about 0.70 to 1.2. Reynolds numbers for these tests, based on vertical-tail-panel mean aerodynamic chord, varied from 8.4×10^6 to 13.2×10^6.

The control inputs and the subsequent airplane motions and measured loads for each type maneuver performed are illustrated by the time histories shown in figures 3 to 5.

RESULTS AND DISCUSSION

Vertical-Tail Loads

The rudder-pulse maneuvers performed during this investigation, as shown in figure 3 for the maneuver made at $M = 0.93$, consisted of an abrupt displacement of the rudder to peak deflection before appreciable sideslip had developed, followed by an abrupt return of the rudder to neutral or near neutral. Following this type of control input, a lateral-directional oscillation resulted with rudder held constant. Variations of vertical-tail side-force coefficient, bending-moment coefficient, and torque coefficient associated with rudder deflections were obtained from the initial portion of the maneuver where sideslip was constant. These variations are shown in figure 6 for Mach numbers of 0.93 and 1.14. The variation of vertical-tail side-force coefficient with rudder position $\frac{dC_{Y_V}}{d\delta_r}$ was determined in this manner for each test Mach number. During the oscillations which followed the rudder pulses, variations with sideslip angle of vertical-tail side-force, bending-moment, and torque coefficients were determined and are shown in figure 7 for the maneuvers performed at $M = 0.93$ and 1.14. The variation of vertical-tail side-force coefficient with sideslip angle $\frac{dC_{Y_V}}{d\beta}$ during the oscillations was considered to be the vertical-tail lift-curve slope.

Another type maneuver, the rudder-fixed aileron roll, performed during this investigation also resulted in sideslip response of the airplane. Variations of vertical-tail side-force, bending-moment, and torque coefficients with sideslip angle during an aileron roll at $M = 0.90$ are shown in figure 8. In this figure the variation of vertical-tail load with sideslip angle, which is typical of the data obtained in the roll maneuvers, is essentially linear, indicating that the effects on the vertical-tail loads of the rolling and yawing motions encountered during these maneuvers are of a secondary nature. Therefore, data from several roll maneuvers throughout the test Mach number range were also used to determine the variation of vertical-tail side-force coefficient with sideslip angle.

The variation with Mach number of $\frac{dC_{Y_V}}{d\delta_r}$ and $\frac{dC_{Y_V}}{d\beta}$ obtained from both the rudder-pulse and aileron roll maneuvers is shown in figure 9. A reduction in effectiveness of the rudder to produce side force on the vertical tail from a value of $\frac{dC_{Y_V}}{d\delta_r} = 0.020$ per degree at subsonic Mach numbers to 0.013 at Mach numbers above 1.0 is shown in figure 9. The lift-curve slope of the vertical tail increases with Mach number from a value of 0.038 at low Mach numbers to a peak of 0.048 at $M = 0.94$, followed by a reduction to 0.041 at supersonic Mach numbers.

The dashed curve in figure 9 (labeled "estimated") is the vertical-tail lift-curve slope obtained by using the charts of reference 7. Before using the charts, however, a value of effective aspect ratio was determined. The vertical-tail panel (portion of the vertical tail outboard of the strain gages) has a geometric aspect ratio of 1.18. This value of geometric aspect ratio was increased by 55 percent (ref. 8) to account for the end-plate effect of the horizontal tail and fuselage, resulting in an effective aspect ratio of 1.83. The curves of reference 7 for an aspect ratio of 1.83 and sweep of the quarter chord of 40° yield a value of $C_{L_\alpha} = 0.038$ for the lift-curve slope at $M = 0$. The modified Prandtl-Glauert factor was employed to account for compressibility effects and resulted in the increase in lift-curve slope with Mach number shown by the dashed line in figure 9. Good agreement is indicated between the flight measurements and the estimated vertical-tail lift-curve slope.

The data points presented in figure 9 were determined from measurements made at sideslip angles less than about 6°. In several roll maneuvers made at two Mach numbers, 0.92 and 1.05, however, large sideslip angles were encountered. A time history of the vertical-tail side-force coefficients and other pertinent data is reproduced in figure 10 for a maneuver where a sideslip angle of 21° was reached at $M = 1.05$ at about 25,000 feet. The dashed line in figure 10 (labeled "calculated") was obtained by using the value of $\frac{dC_{Y_V}}{d\beta}$ of 0.042 and $\frac{dC_{Y_V}}{d\delta_r}$ of 0.013 from figure 9 corresponding to $M = 1.05$ and multiplying these coefficients by the measured sideslip angles and rudder positions. The calculations deviate from the experimental data when a sideslip angle of approximately 12° is exceeded, indicating that the vertical tail suffers a loss in effectiveness above this angle of sideslip. The discrepancy between measured vertical-tail side-force coefficients and calculations based on the coefficients derived from small sideslip angle data was found to occur at about 12° wherever this sideslip angle was exceeded.

In an attempt to account for this indicated reduction in effectiveness, wing-span loadings from unpublished pressure measurements obtained simultaneously with the vertical-tail strain-gage data were examined for indications of abrupt changes in wing-span loading near the inboard portion of the wings. Inspection of the wing-span loadings, however, did not show evidence of any changes which were consistent with changes in sideslip angle and which might be correlated with the loss in effectiveness of the vertical tail as indicated by the reduction of side-force coefficient with sideslip. Therefore, the effectiveness is apparently modified by flow conditions at the tail, which are the result of interference effects (rear fuselage and engine wake, for example) rather than effects which emanate from the wings.

Center of Pressure

Variations of the bending-moment and torque coefficients with side-force coefficient during the initial portion of a rudder-pulse maneuver and during the sideslip oscillations following the pulse are shown in figure 11 for a maneuver at $M = 0.93$. Similar variations are shown in figure 12 for a roll maneuver at $M = 0.90$. Slopes of the lines faired through these data yield the center of pressure of the load outboard of the strain-gage measurement station $\frac{dC_{b_V}}{dC_{Y_V}}$ and about the quarter chord of the vertical-tail-panel mean aerodynamic chord $\frac{dC_{T_V}}{dC_{Y_V}}$. Values of $\frac{dC_{b_V}}{dC_{Y_V}}$ and $\frac{dC_{T_V}}{dC_{Y_V}}$ obtained from the pulse portion of the maneuver where sideslip was constant gave the center of pressure due to displacing the rudder. The center of pressure due to sideslip was determined from the oscillations in sideslip with rudder held steady in both the pulse and roll maneuvers. Centers of pressure were obtained in a similar manner from data at each test Mach number and the variations with Mach number of the spanwise and chordwise centers of pressure are presented in figure 13. The circular symbols of figure 13 are the data from the oscillations in sideslip following the rudder pulses and in the aileron roll maneuvers; the square symbols are the data from the rudder-deflected portion of the pulse maneuver with sideslip constant. In sideslip with rudder constant, little change with Mach number is noted for the spanwise center of load which is about 55 percent of the panel span. The chordwise center of pressure remained essentially constant with Mach number at about 30 percent panel mean aerodynamic chord except at the highest test Mach number. These data were obtained in maneuvers where maximum sideslip angles reached were about 6°. During roll maneuvers made at $M = 0.92$ and $M = 1.05$, sideslip angles in excess of 6° were

encountered. The variations of C_{b_V} and C_{T_V} with C_{Y_V} for these maneuvers are presented in figure 14. It can be seen from this figure that extension to the higher sideslip angles shows that the variation of C_{T_V} with C_{Y_V} became nonlinear in such a way that a more rearward chordwise center of pressure is indicated.

The center of load associated with deflecting the rudder at constant sideslip is farther inboard, 45 percent of the panel span, than the spanwise center of load due to sideslip. Chordwise, the rudder-deflected load center is 63 percent of the chord from the leading edge and moves rearward to about 85 percent of the chord at supersonic Mach numbers.

Variation of Yawing-Moment Coefficient With Sideslip

In these maneuvers, the load on the vertical-tail surface acting a distance l_V rearward of the center of gravity of the airplane, may be approximated by a component associated with yawing acceleration and a component which balances the yawing moment of the airplane less vertical tail. This relationship can be expressed as

$$L_V l_V = C_{n_{\beta_{wf}}} \beta q S b - I_Z \dot{r}$$

During a steady sideslip maneuver with zero yawing angular acceleration, the vertical-tail load is a measure of the wing-fuselage yawing-moment coefficient in sideslip. In the sideslip maneuvers performed during this investigation, steady sideslip maneuvers were approximated since the sideslip angle was increased gradually and the resulting yawing accelerations were small. Representative data are shown in figure 15 for sideslips made at Mach numbers of approximately 0.75 and 0.92 where the rudder required to balance the airplane in sideslipping flight and the resulting vertical-tail side-force, bending-moment, and torque coefficients are shown. Variations of vertical-tail side-force coefficient with sideslip angle as shown in figure 15 were obtained from all sideslip maneuvers, and variations of $\frac{dC_{Y_V}}{d\beta}$ with Mach number are presented in figure 16. The variation of the yawing-moment coefficient of the wing-fuselage with sideslip was then evaluated from the expression

$$C_{n_{\beta_{wf}}} = \frac{dC_{Y_V}}{d\beta} \frac{S_V}{S} \frac{l_V}{b}$$

and the variation with Mach number of $C_{n_{\beta_{wf}}}$ is shown in figure 17. It can be seen that the wing-fuselage becomes slightly more unstable as $M = 1.0$ is approached, with a reversal of this trend at supersonic speeds. The sideslip maneuvers from which the data of figure 17 were obtained were performed with variable aileron deflections, and $C_{n_{\beta_{wf}}}$ presented in the figure contains the yawing-moment contribution from the ailerons. The data, however, have not been modified to take into account the effect of the ailerons, since available data for the test airplane configuration indicate that yawing moments contributed by the ailerons are small and can be neglected for the flight conditions of the present investigation. Also shown in figure 17 is the variation of the yawing-moment coefficient with sideslip contributed by the vertical tail as determined by substituting values of $\frac{dC_{Y_V}}{d\beta}$, obtained from the pulse oscillations and roll maneuvers and given in figure 12, in the expression

$$C_{n_{\beta_V}} = \frac{S_V}{S} \frac{l_V}{b} \left(\frac{dC_{Y_V}}{d\beta} \right)_{\delta_r=0}$$

This parameter increases with increasing Mach number to $M = 0.95$, and experiences a reduction thereafter similar to the data of figure 9.

The sum of $C_{n_{\beta_V}}$ and $C_{n_{\beta_{wf}}}$ results in C_{n_β} of the complete airplane. This value is shown in figure 17 by the solid curve. Values of C_{n_β} vary from 0.0023 per degree at $M = 0.7$ to 0.0032 at $M = 0.94$, then drop off again to a value of 0.0023.

The rudder displacements required to balance the airplane in sideslipping flight have been determined for each test Mach number from the variations of rudder position with sideslip angle as indicated in figure 15 for $M = 0.75$ and 0.92. The results for these and the other test Mach numbers are summarized in figure 16 in which the variation with Mach number of the sideslip angle associated with rudder position $\frac{d\beta}{d\delta_r}$ is shown. A progressive loss in rudder effectiveness as Mach number is increased is indicated in figure 16.

CONCLUSIONS

Analysis of the measurements of vertical-tail loads made during a flight investigation of the Douglas X-3 research airplane has indicated:

1. The effective vertical-tail lift-curve slope determined from sideslip oscillations following rudder-pulse maneuvers and in rudder-fixed rolls increased with increasing Mach number from a value of 0.038 at low Mach numbers to a peak of 0.048 at a Mach number of 0.94, followed by a reduction to 0.041 at supersonic Mach numbers. Estimates of this parameter based on published span loading data and estimates of horizontal-tail and fuselage end-plate effects indicate good agreement with the flight results.

2. In several violent roll maneuvers, large sideslip angles were reached (21°) without stalling of the vertical tail, although the lift effectiveness was reduced above about 12° sideslip.

3. Rudder effectiveness parameter $\frac{dC_{Y_V}}{d\delta_r}$ as determined from rudder-pulse data, decreased from approximately 0.020 per degree at subsonic Mach numbers to 0.013 per degree at supersonic Mach numbers.

4. The center of pressure of load on the vertical tail in sideslip was practically unchanged with Mach number, remaining at about 55 percent span and 30 percent chord at sideslip angles below about 6°. At sideslip angles above this value the variation of the vertical-tail-panel torque coefficient C_{T_V} with the vertical-tail-panel side-force coefficient C_{Y_V} became nonlinear in such a way that a more rearward chordwise center of pressure was indicated. The center of pressure due to displacing the rudder was farther inboard, 45 percent span, and farther rearward, 63 percent chord, than in sideslip and moved rearward to 85 percent chord at supersonic Mach numbers.

5. The variation of airplane yawing-moment coefficient with sideslip C_{n_β} as determined from vertical-tail-loads measurements, increased

from 0.0023 per degree at a Mach number of 0.70 to a maximum of 0.0032 at a Mach number of 0.94 and decreased to 0.0023 at supersonic Mach numbers.

High-Speed Flight Station,
National Advisory Committee for Aeronautics,
Edwards, Calif., July 30, 1956.

REFERENCES

1. Bellman, Donald R., and Murphy, Edward D.: Lift and Drag Characteristics of the Douglas X-3 Research Airplane Obtained During Demonstration Flights to a Mach Number of 1.20. NACA RM H54I17, 1954.

2. Day, Richard E., and Fischel, Jack: Stability and Control Characteristics Obtained During Demonstration of the Douglas X-3 Research Airplane. NACA RM H55E16, 1955.

3. NACA High-Speed Flight Station: Flight Experience With Two High-Speed Airplanes Having Violent Lateral-Longitudinal Coupling in Aileron Rolls. NACA RM H55A13, 1955.

4. Stephenson, Harriet J.: Flight Measurements of Horizontal-Tail Loads on the Douglas X-3 Research Airplane. NACA RM H56A23, 1956.

5. Jordan, Gareth H., and Hutchins, C. Kenneth, Jr.: Preliminary Flight-Determined Pressure Distributions Over the Wing of the Douglas X-3 Research Airplane at Subsonic and Transonic Mach Numbers. NACA RM H55A10, 1955.

6. Keener, Earl R., and Jordan, Gareth H.: Wing Loads and Load Distributions Throughout the Lift Range of the Douglas X-3 Research Airplane at Transonic Speeds. NACA RM H56G13, 1956.

7. DeYoung, John, and Harper, Charles W.: Theoretical Symmetric Span Loading at Subsonic Speeds for Wings Having Arbitrary Plan Form. NACA Rep. 921, 1948.

8. Pass, H. R.: Analysis of Wind-Tunnel Data on Directional Stability and Control. NACA TN 775, 1940.

TABLE I

PHYSICAL CHARACTERISTICS OF THE DOUGLAS X-3 AIRPLANE

Wing:	
Airfoil section	Modified hexagon
Airfoil thickness ratio, percent chord	4.5
Total area, sq ft	166.50
Span, ft	22.69
Mean aerodynamic chord, ft	7.84
Taper ratio	0.39
Aspect ratio	3.09
Sweep of 75 percent chord line, deg	0
Incidence, deg	0
Dihedral, deg	0
Geometric twist, deg	0
Horizontal tail:	
Airfoil section	Modified hexagon
Airfoil thickness ratio at root chord, percent chord	8.01
Airfoil thickness ratio outboard of station 26, percent chord	4.50
Total area, sq ft	43.24
Span, ft	13.77
Mean aerodynamic chord, ft	3.34
Taper ratio	0.405
Aspect ratio	4.38
Sweep at leading edge, deg	21.14
Sweep at trailing edge, deg	0
Dihedral, deg	0
Travel, leading edge up, deg	6
Travel, leading edge down, deg	17
Hinge-line location, percent root chord	46.46
Vertical tail:	
Airfoil section	Modified hexagon
Airfoil thickness ratio, percent chord	4.5
Area, sq ft	23.73
Span, ft	5.59
Mean aerodynamic chord, ft	4.69
Root chord, ft	6.508
Tip chord, ft	1.93
Taper ratio	0.292
Aspect ratio	1.315
Sweep of leading edge, deg	45
Sweep of trailing edge, deg	9.39
Rudder:	
Area, rearward of hinge line, sq ft	5.44
Span at hinge line, ft	3.535
Root chord, ft	1.98
Tip chord, ft	1.097
Travel, deg	±20
Vertical-tail panel (outboard of strain-gage reference station):	
Area, sq ft	17.05
Span, ft	4.48
Mean aerodynamic chord, ft	4.11
Root chord, ft	5.68
Tip chord, ft	1.93
Taper ratio	0.341
Aspect ratio	1.18
Fuselage:	
Length including boom, ft	66.75
Maximum width, ft	6.08
Maximum height, ft	4.81
Base area, sq ft	7.94
Airplane weight, lb:	
Basic (without fuel, oil, water, pilot)	16,120
Total (full fuel, oil, water, no pilot)	21,900
Center-of-gravity location, percent mean aerodynamic chord.	
Basic weight, gear down	2.63
Total weight, gear down	4.59
Total weight, gear up	3.91
Moments of inertia, slug-ft^2 (estimated for total weight):	
I_X	4,100
I_Y	61,200
I_Z	65,100
I_{XZ}	4,200

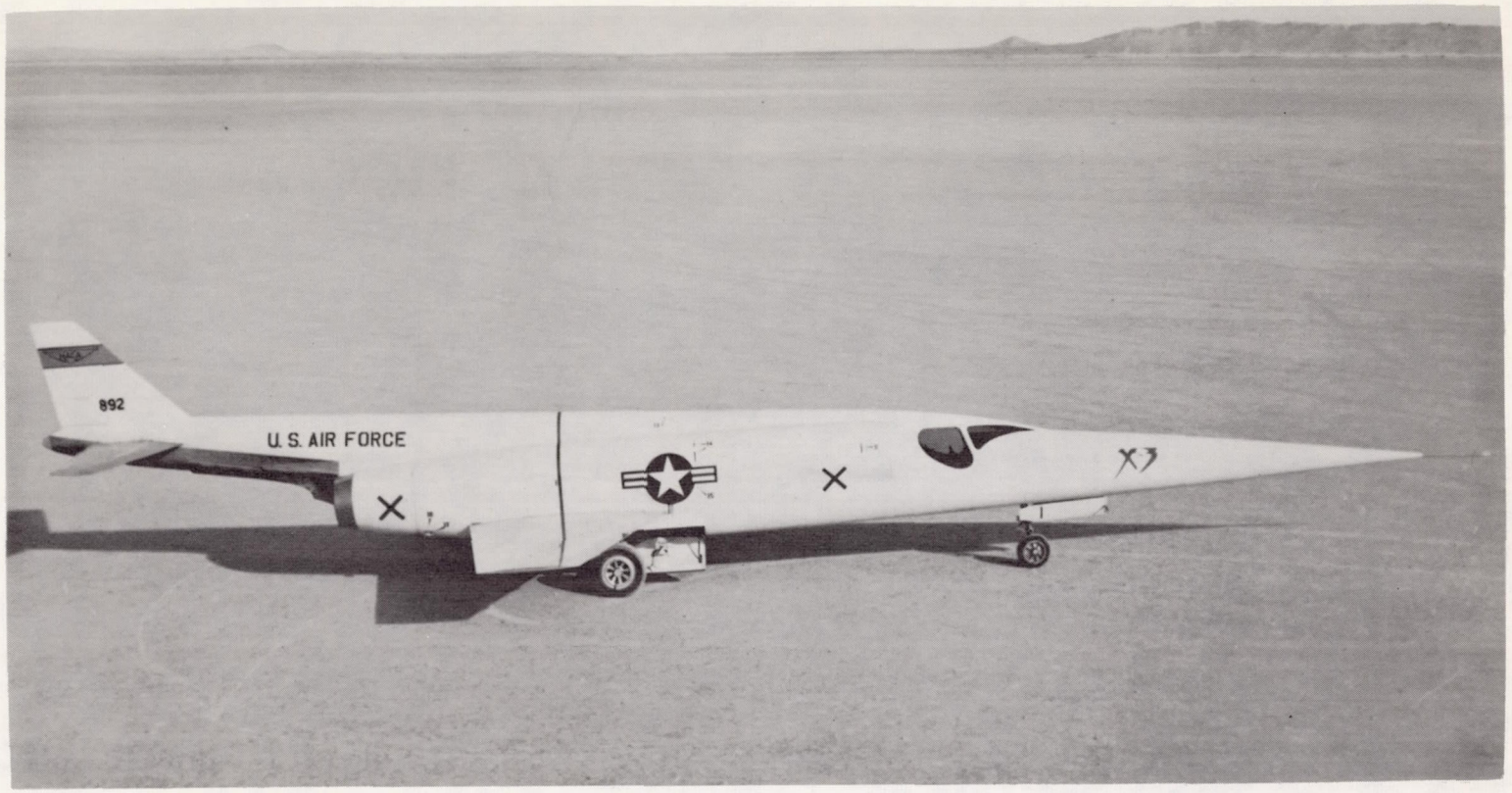

E-1547

Figure 1.- Photograph of the Douglas X-3 research airplane.

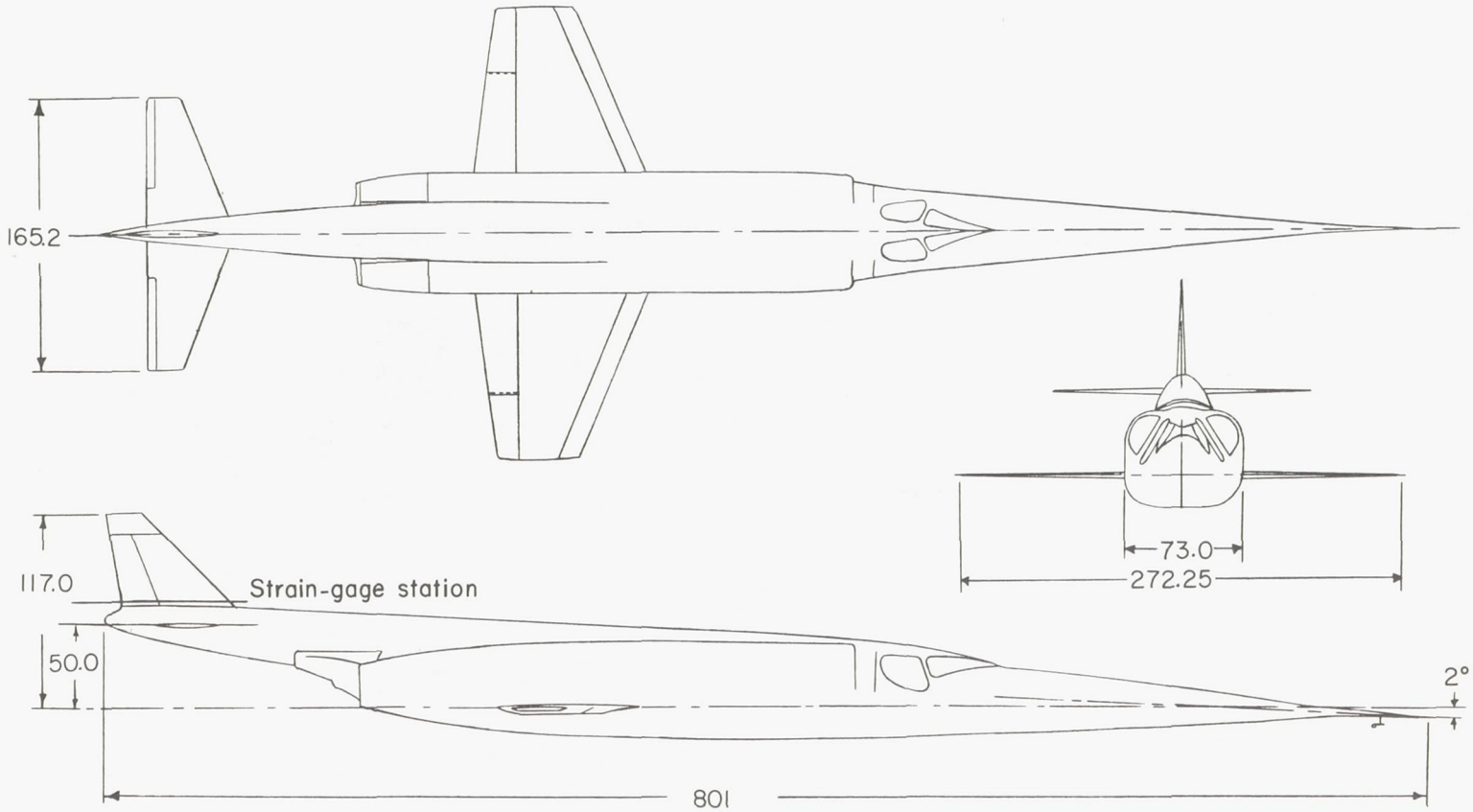

Figure 2.- Three-view drawing of the X-3 airplane. All dimensions in inches.

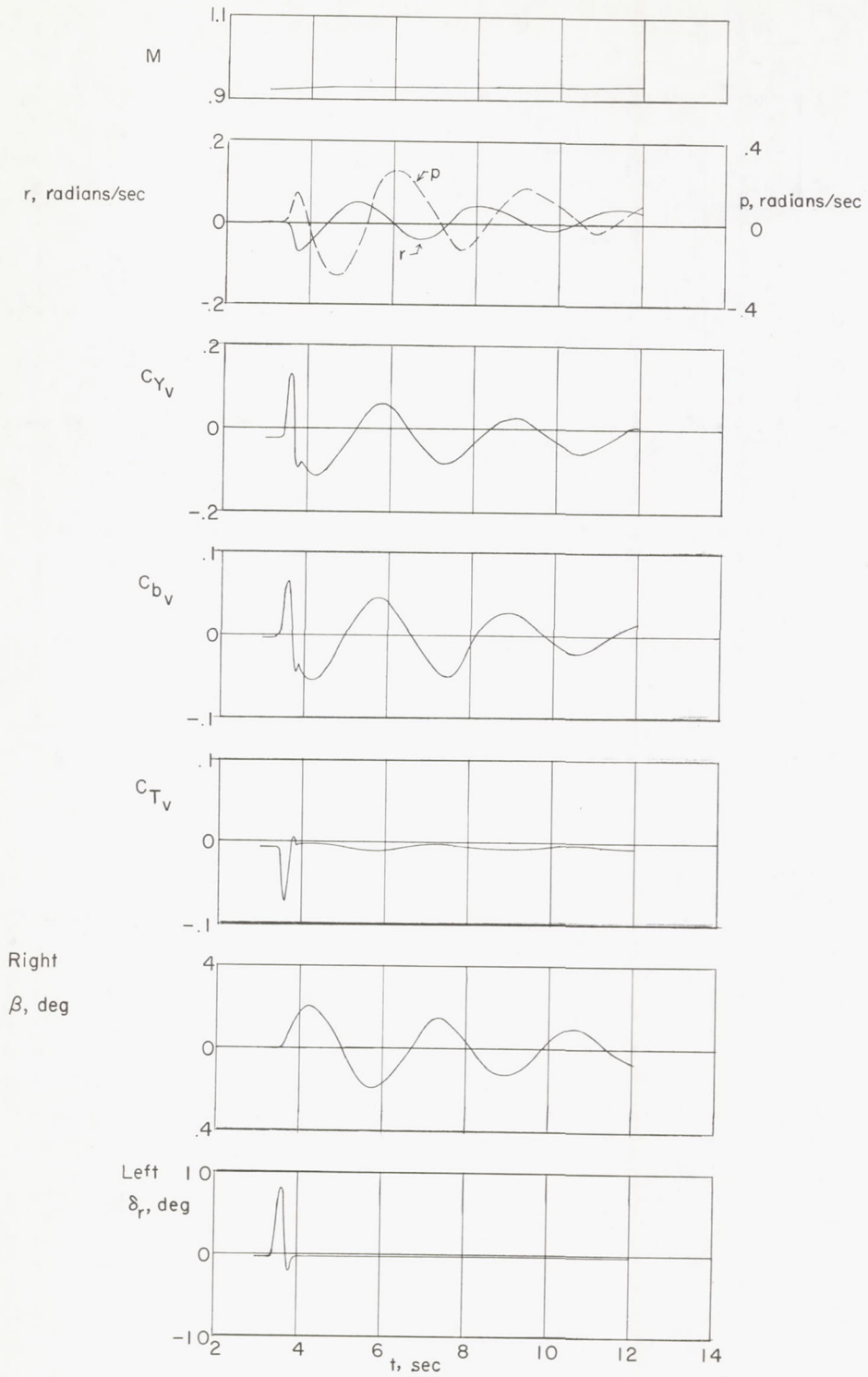

Figure 3.- Time history of the various quantities measured during a rudder-pulse maneuver at M = 0.93 at 30,000 feet.

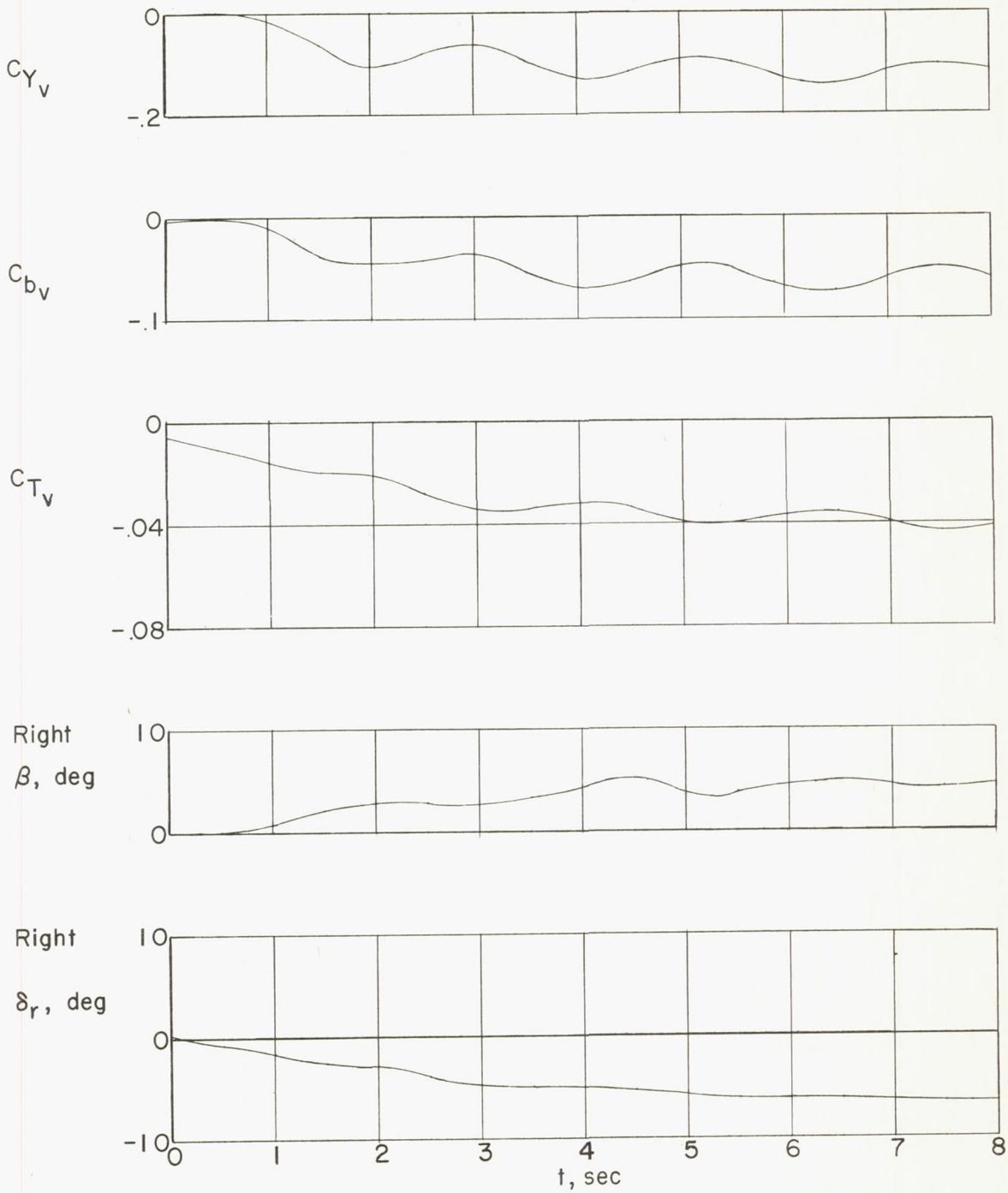

Figure 4.- Time history of the various quantities measured during a steady sideslip maneuver at M = 0.93 at 30,000 feet.

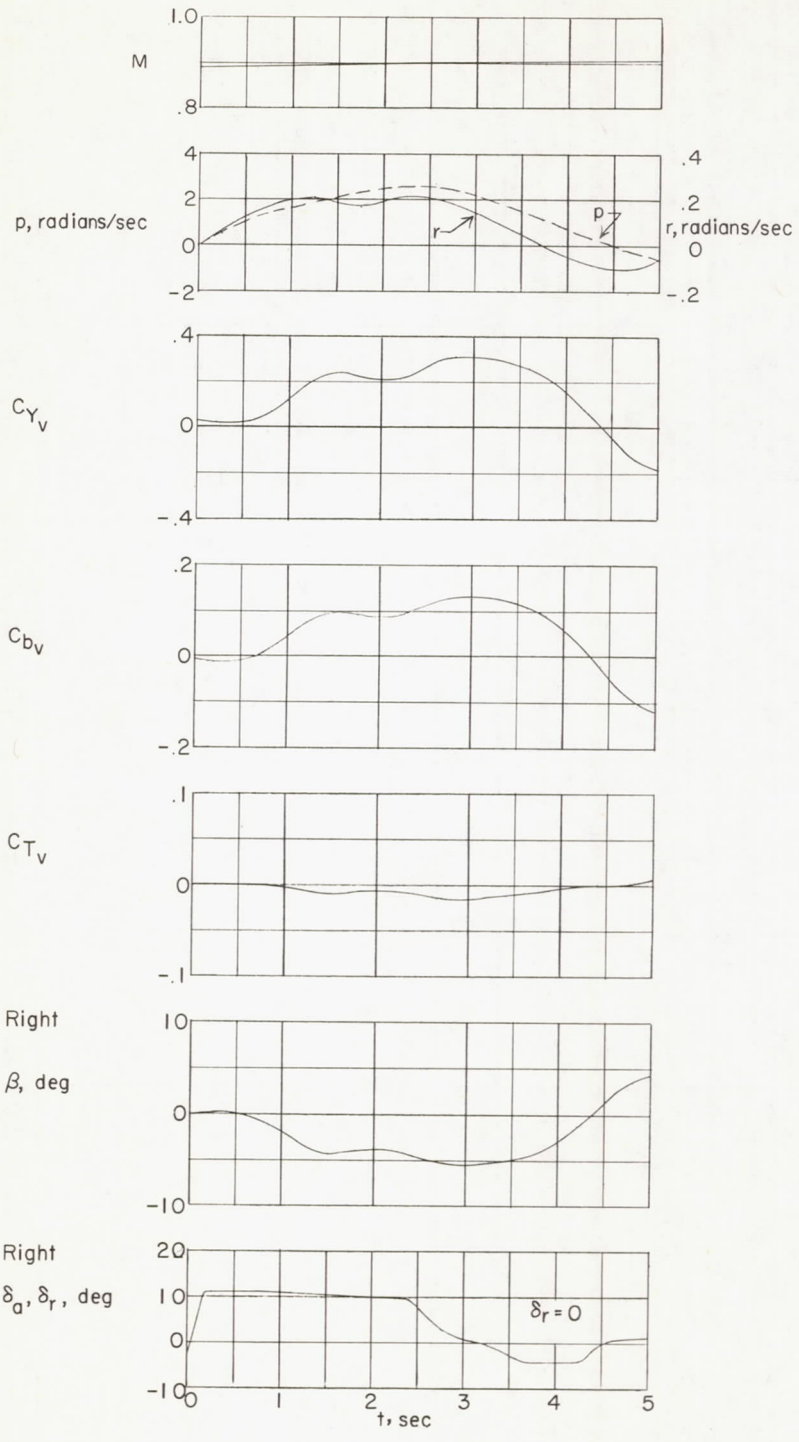

Figure 5.- Time history of the various quantities measured during a rudder-fixed aileron roll maneuver at M = 0.90 at 30,000 feet.

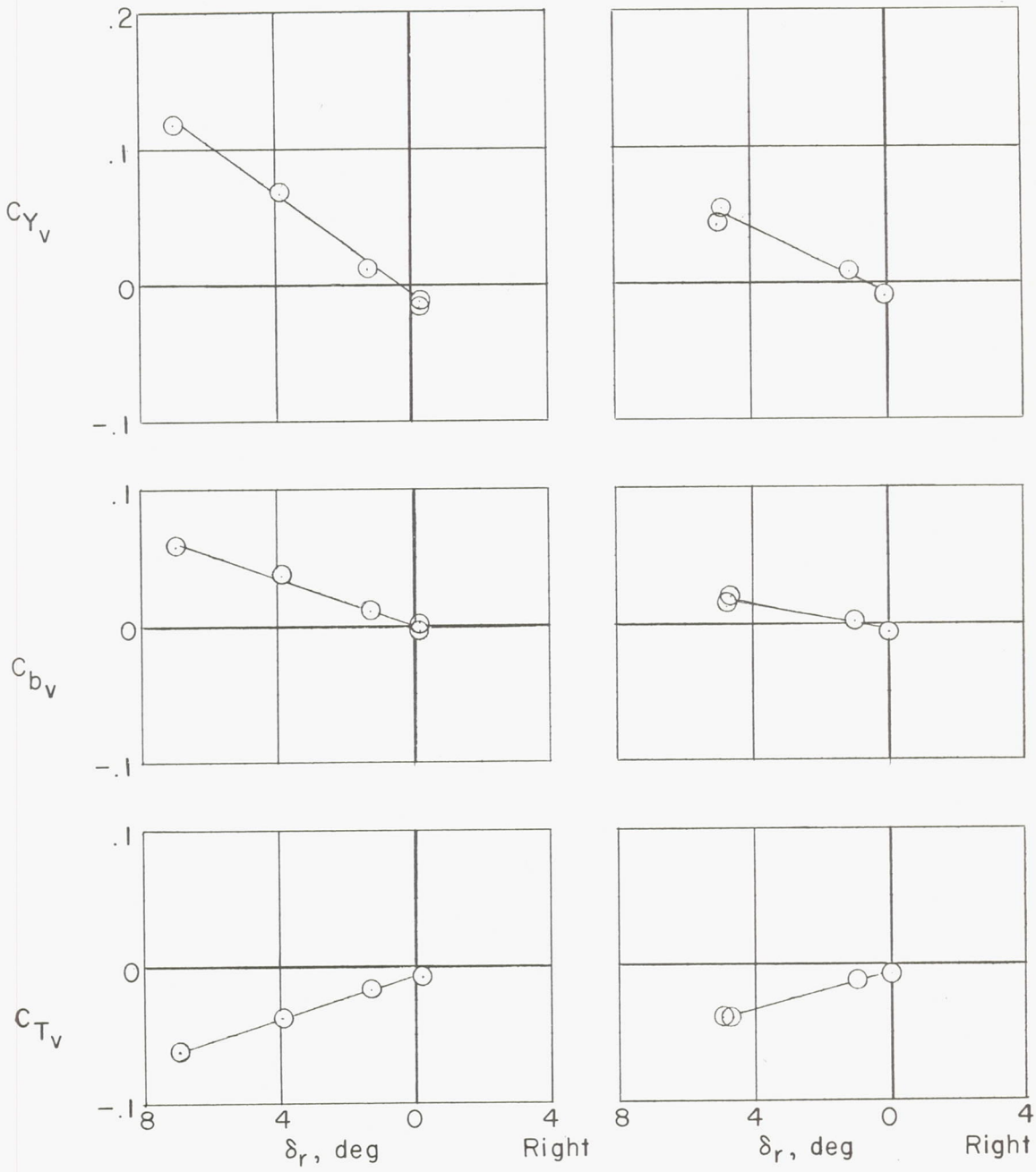

(a) M = 0.93. (b) M = 1.14.

Figure 6.- Variation of vertical-tail side-force, bending-moment, and torque coefficients with rudder position (sideslip angle constant) during rudder-pulse maneuvers at M = 0.93 and 1.14 at 30,000 feet.

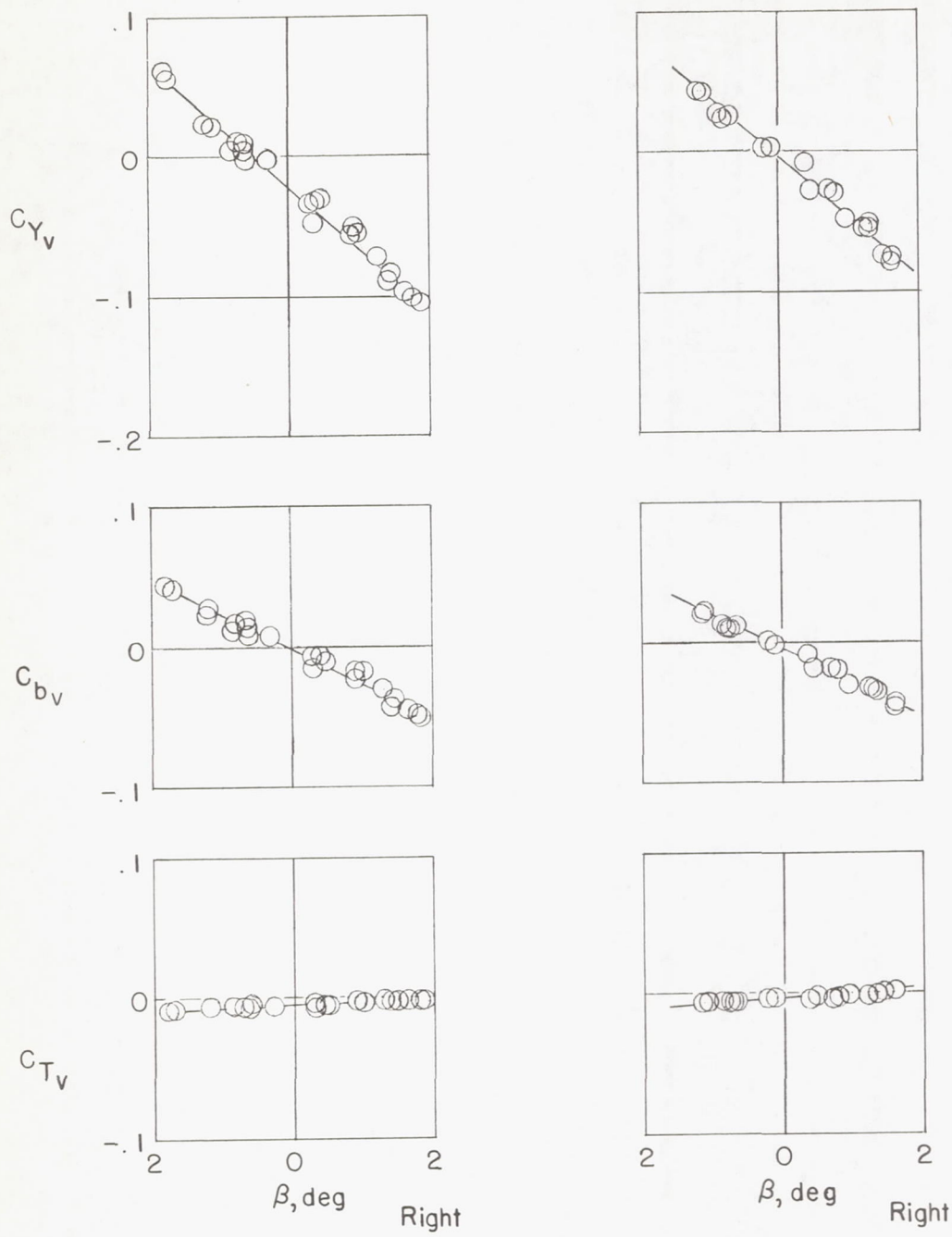

(a) M = 0.93. (b) M = 1.14.

Figure 7.- Variation of vertical-tail side-force, bending-moment, and torque coefficients with sideslip angle (rudder angle constant) during rudder-pulse maneuvers at M = 0.93 and 1.14 at 30,000 feet.

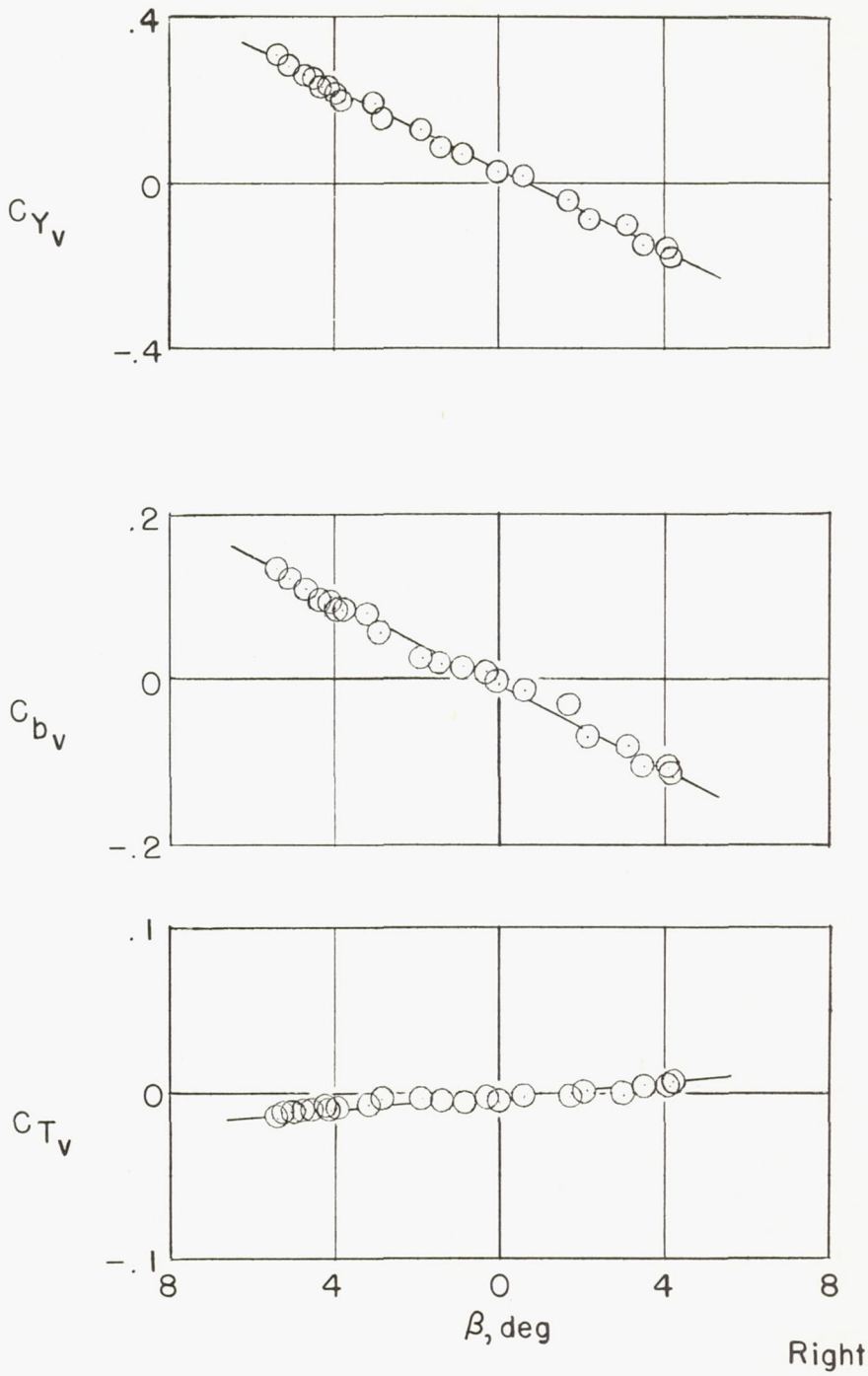

Figure 8.- Variation of vertical-tail side-force, bending-moment, and torque coefficients with sideslip angle (rudder angle constant) during a roll maneuver at M = 0.90 at 30,000 feet.

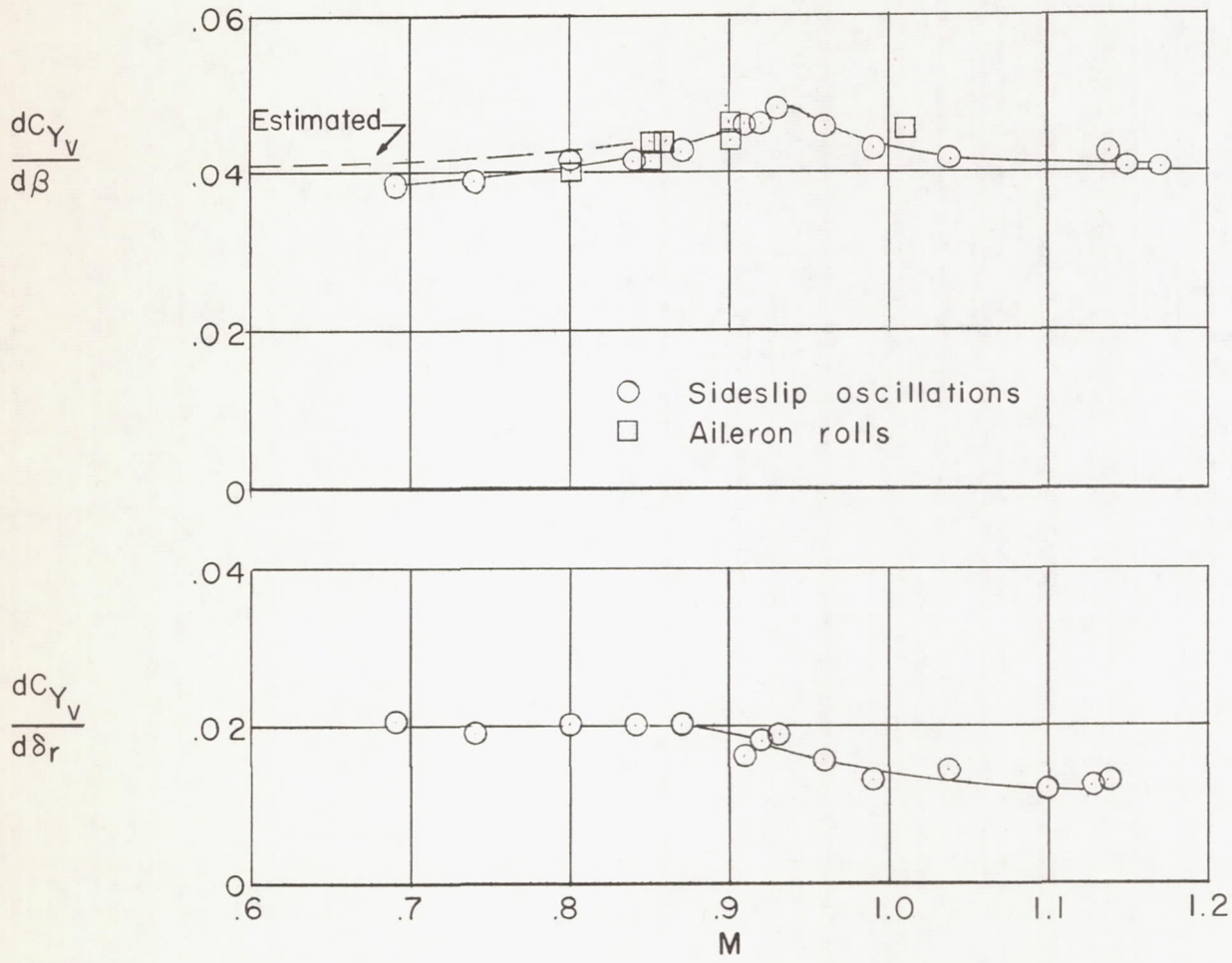

Figure 9.- Variation with Mach number of the vertical-tail side-force coefficient due to sideslip (rudder angle constant) and the vertical-tail side-force coefficient due to rudder position (sideslip angle constant).

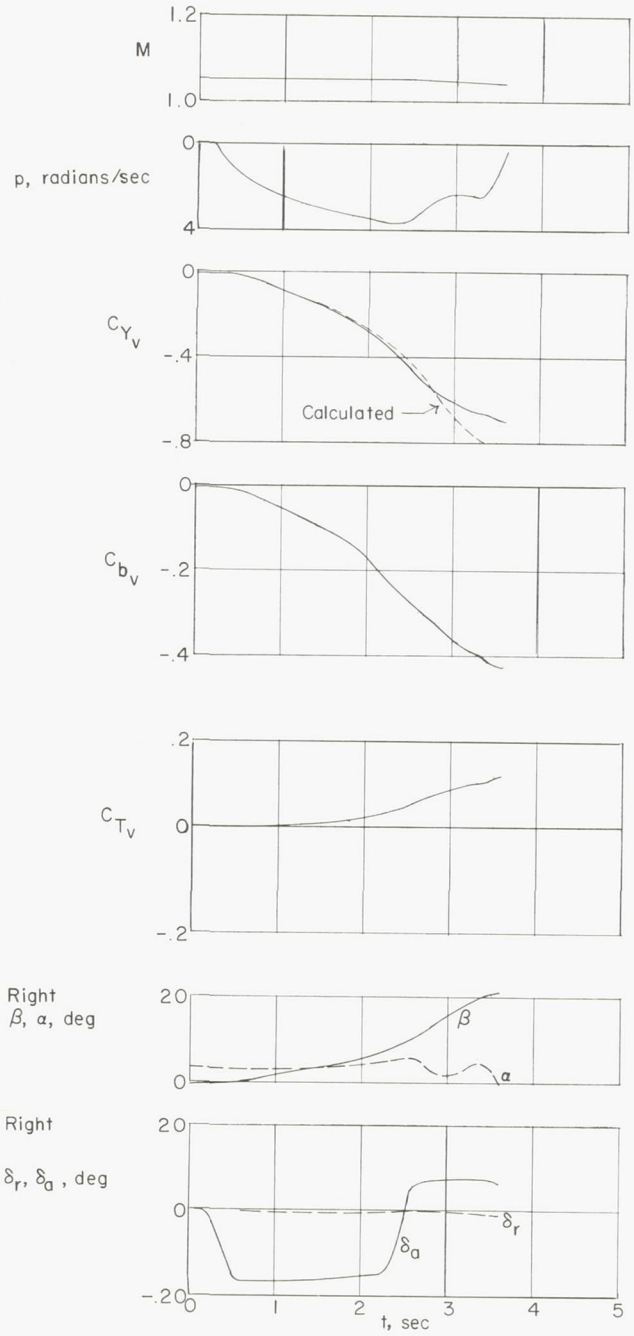

Figure 10.- Time history of the various quantities measured during an aileron roll maneuver at M = 1.05 at 25,000 feet where large sideslip angles were attained.

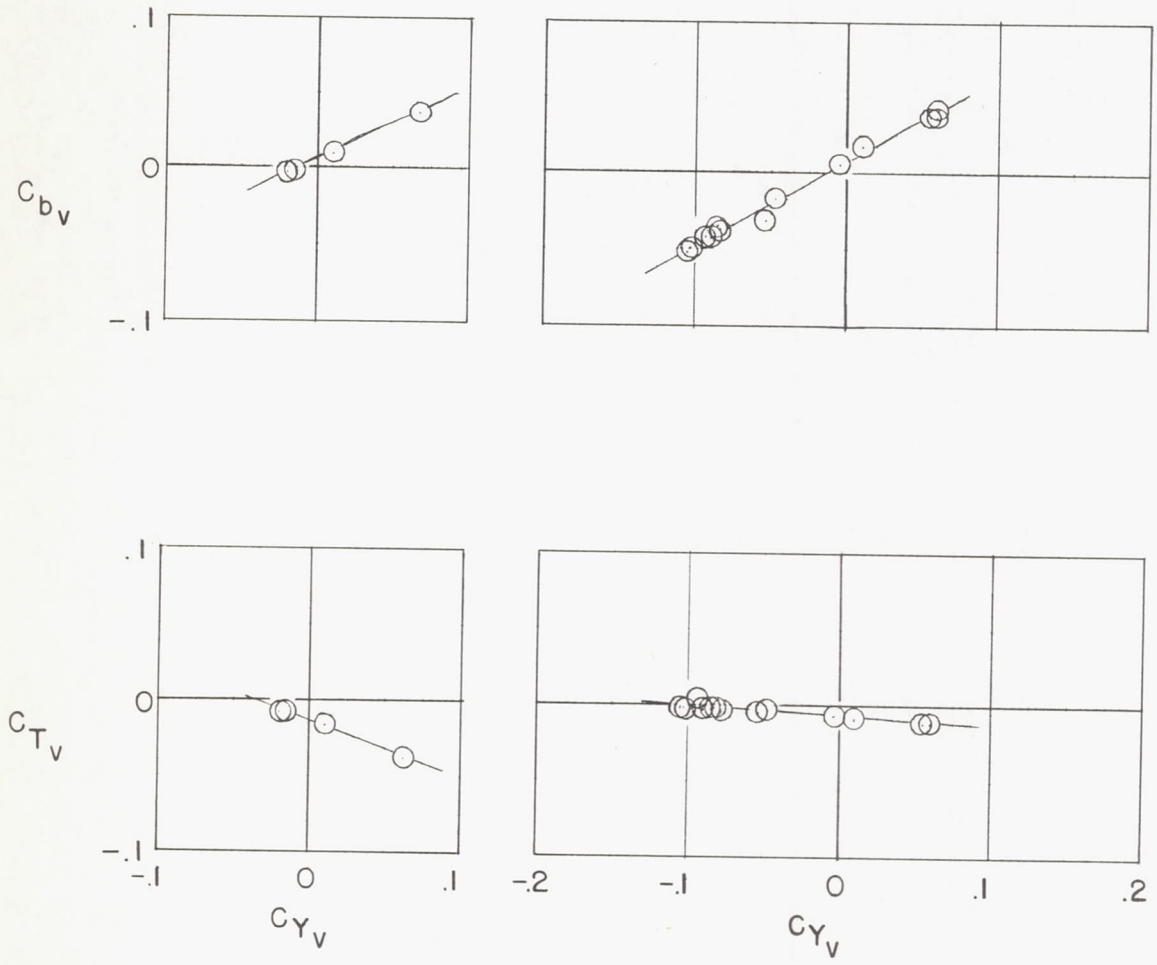

(a) Constant sideslip angle. (b) Constant rudder position.

Figure 11.- Variations with vertical-tail side-force coefficient of the vertical-tail bending-moment and torque coefficients during a rudder-pulse maneuver at M = 0.93 at 30,000 feet.

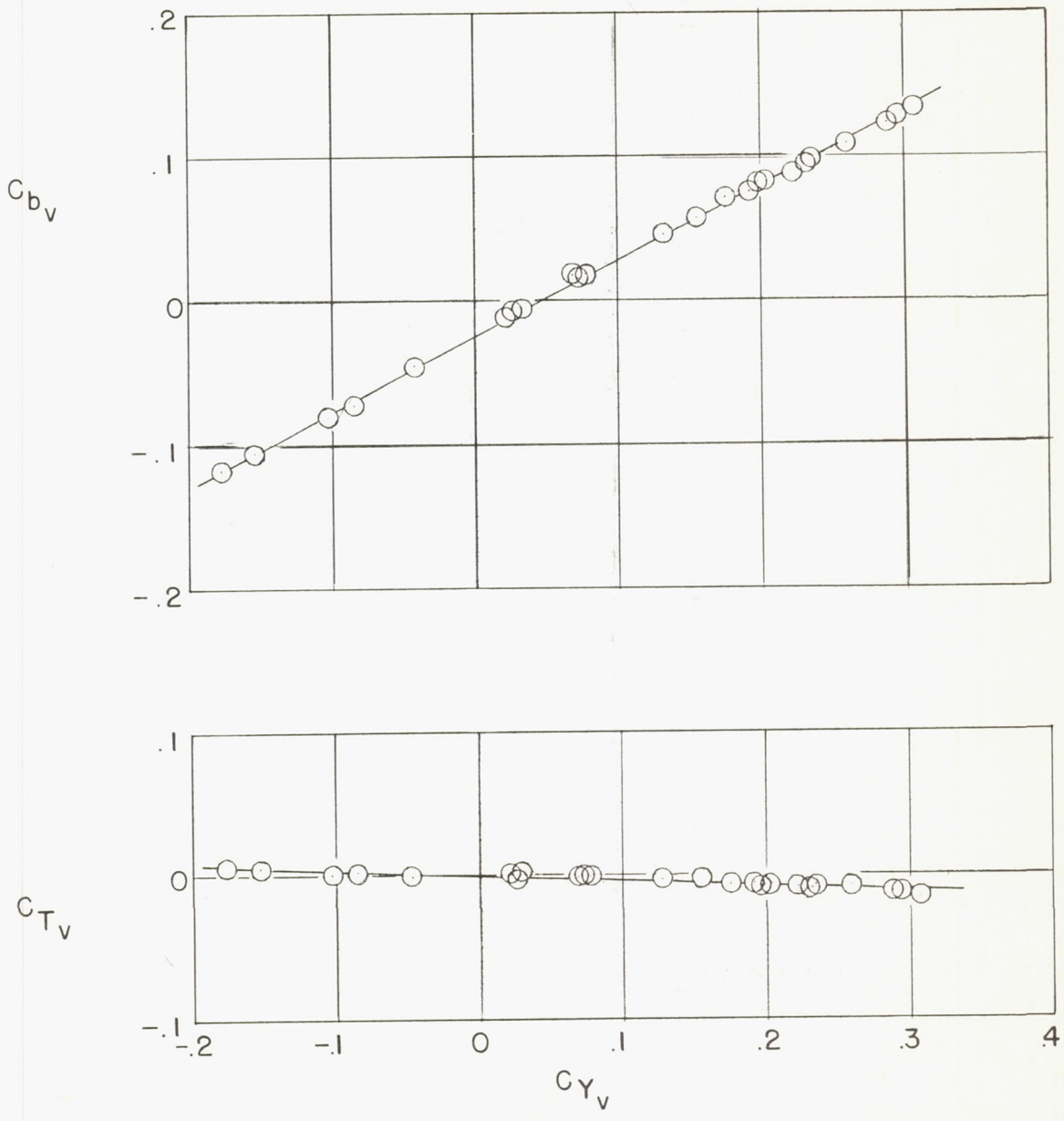

Figure 12.- Variation with vertical-tail side-force coefficient of the vertical-tail bending-moment and torque coefficients during an aileron roll maneuver at M = 0.90 at 30,000 feet.

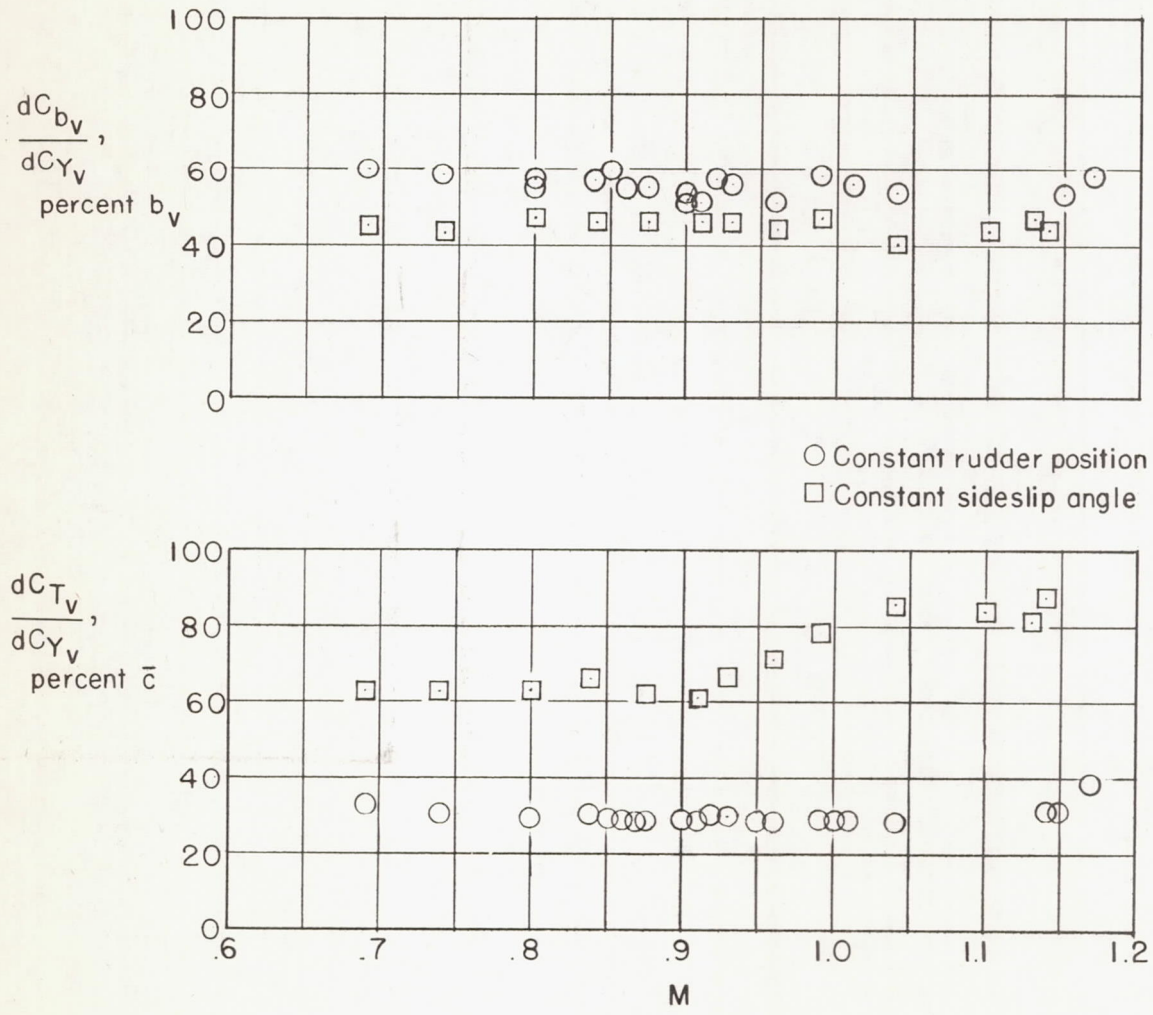

Figure 13.- Variation with Mach number of the center of pressure of the vertical-tail load due to changing sideslip with rudder constant (additional load) and due to displacing the rudder at constant sideslip.

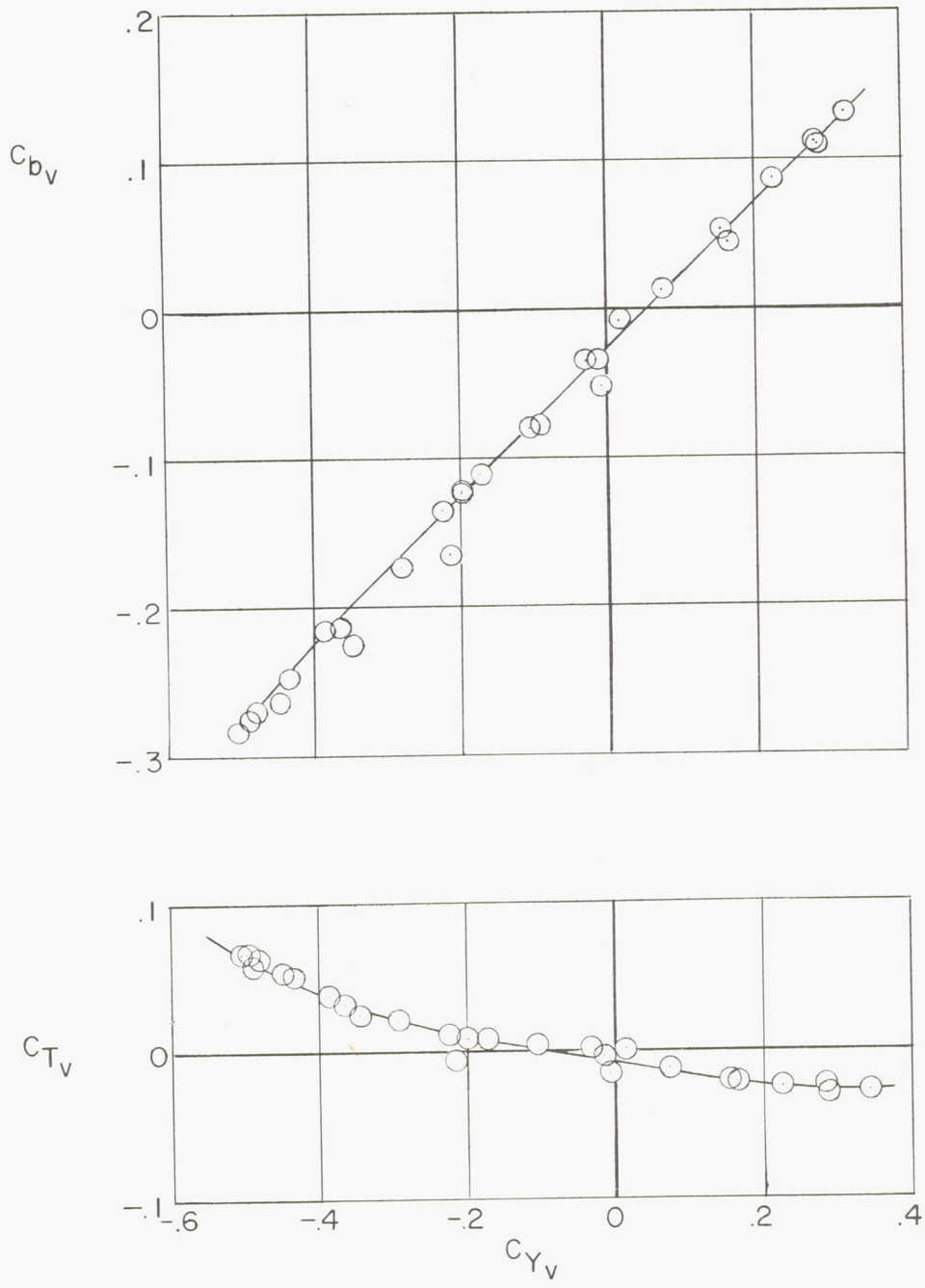

(a) M = 0.92.

Figure 14.- Variation with vertical-tail side-force coefficient of the vertical-tail, bending-moment, and torque coefficients during aileron roll maneuvers.

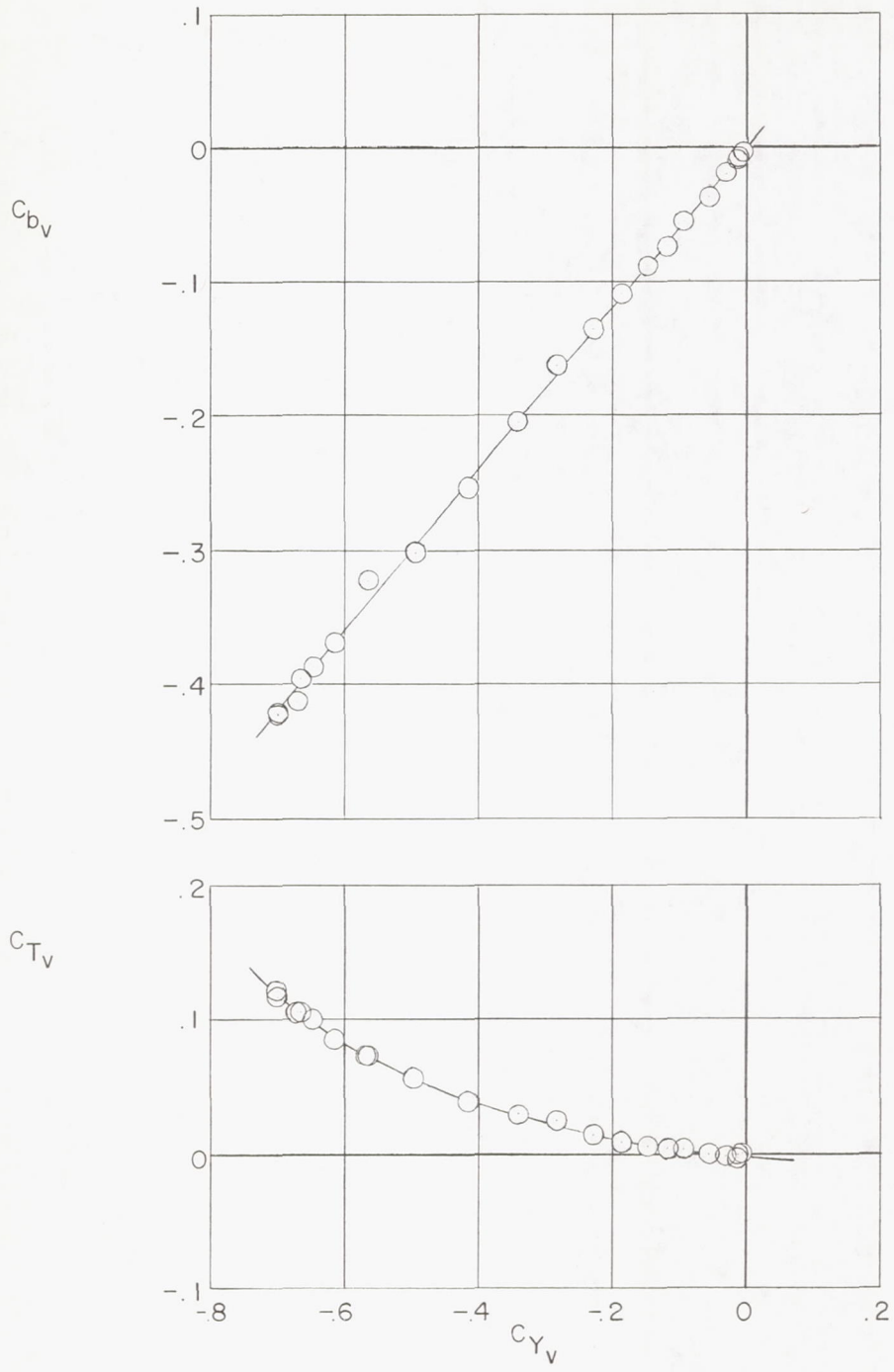

(b) M = 1.05.

Figure 14.- Concluded.

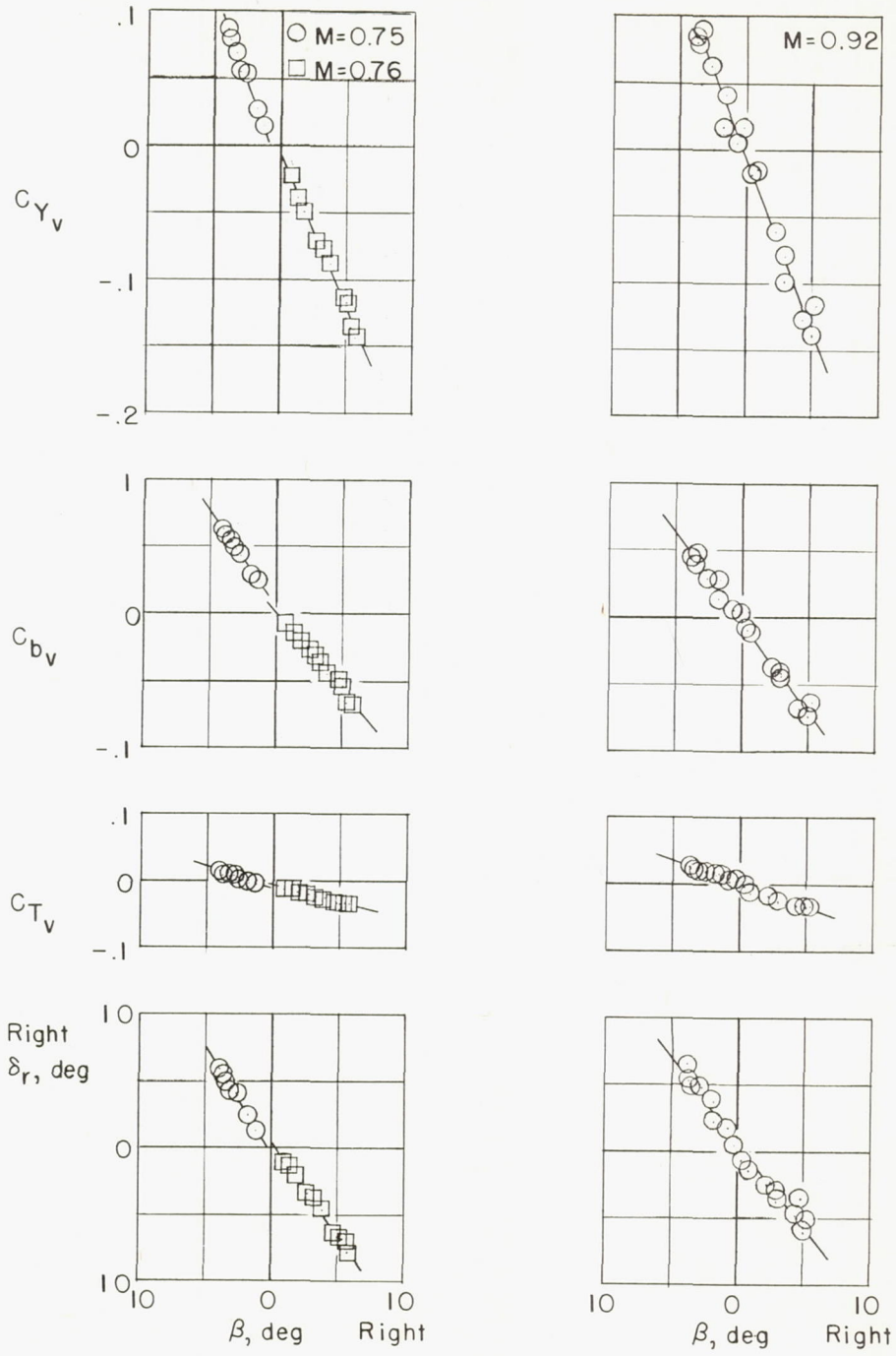

Figure 15.- Variation with sideslip angle of the vertical-tail side-force, bending-moment, and torque coefficients and rudder position in steady sideslip maneuvers at M = 0.75 and 0.92 at 30,000 feet.

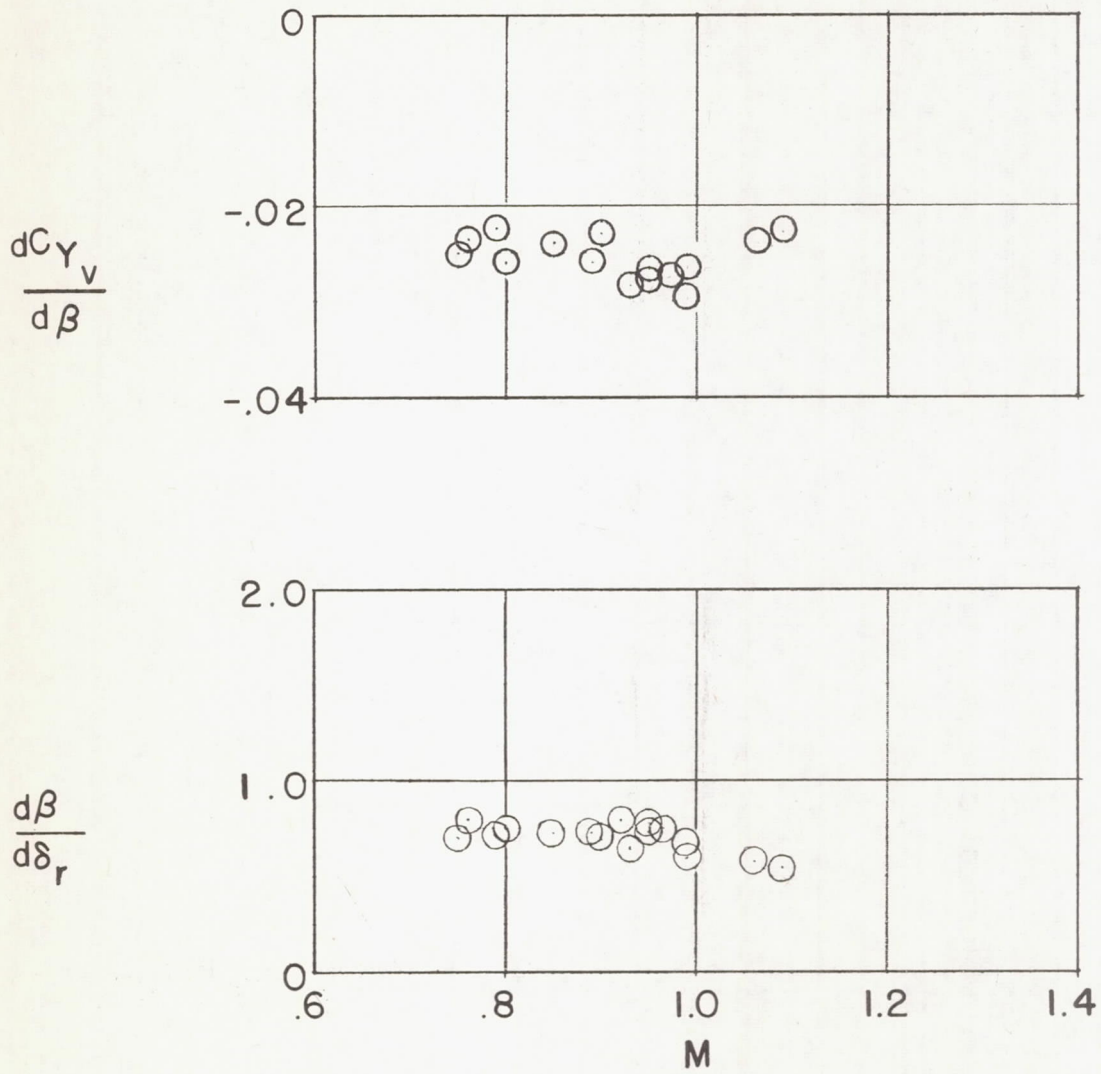

Figure 16.- Variation with Mach number of the vertical-tail side-force coefficient per unit sideslip angle and the sideslip angle for a unit rudder deflection in steady sideslips.

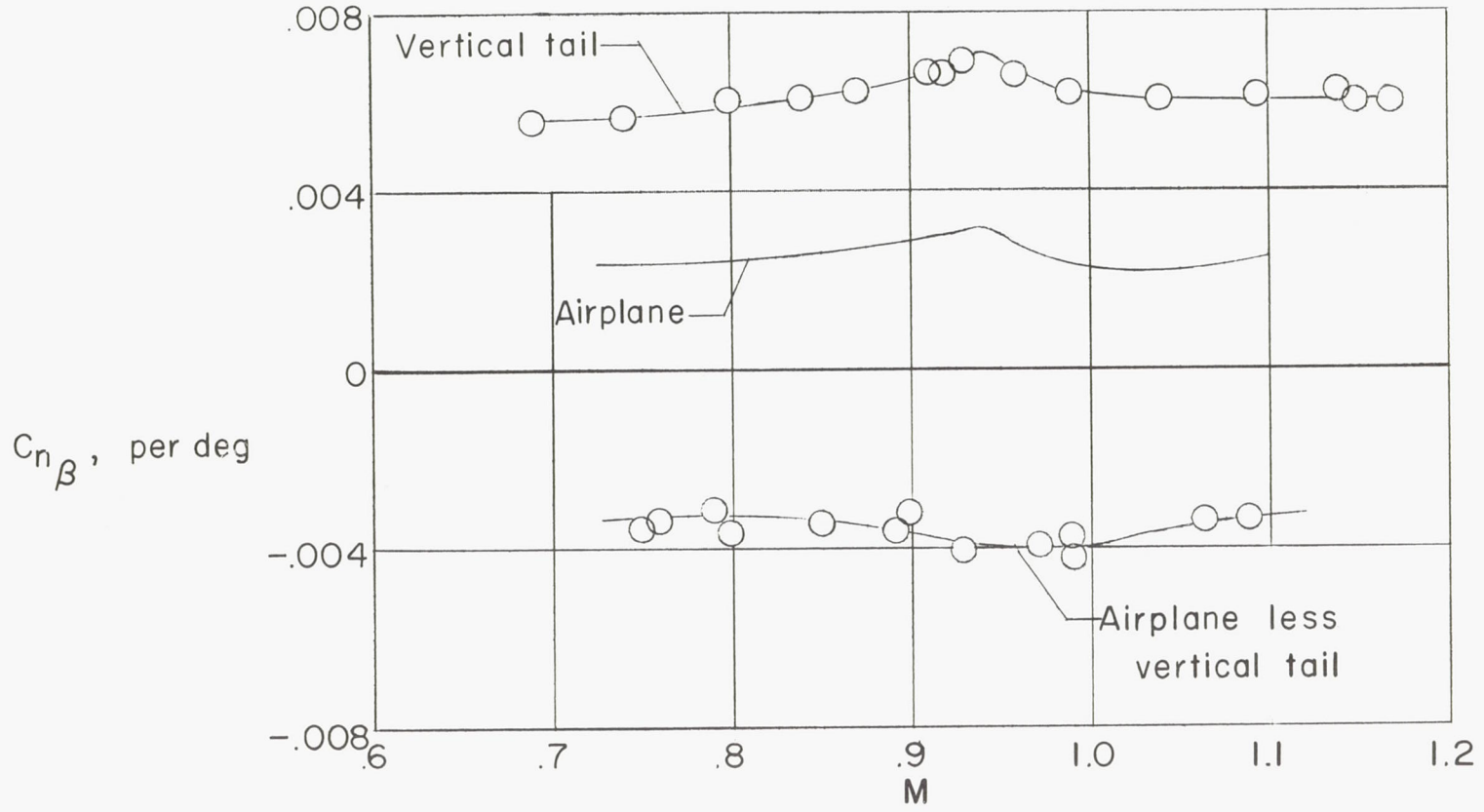

Figure 17.- Variation with Mach number of the yawing-moment coefficient in sideslip of the total airplane and of the component parts of the airplane.

NACA - Langley Field, Va.